Current Bioinformatics, 2011, *6*, 323-343

Mathematical Models and Numerical Schemes for the Simulation of Human Phonation

Fariborz Alipour[1], Christoph Brücker[2], Douglas D. Cook[3], Andreas Gömmel[4], Manfred Kaltenbacher[5], Willy Mattheus[2], Luc Mongeau[6], Eric Nauman[7], Rüdiger Schwarze[2], Isao Tokuda[8] and Stefan Zörner*[,5]

[1]The University of Iowa, National Center for Voice and Speech, Salt Lake City, UT 84101-1623, USA; [2]Institute of Mechanics and Fluid Dynamic, TU Bergakademie Freiberg, Lampadiusstraße 2, 09599 Freiberg, Germany; [3]Mechanical/Biomechanical Engineering, New York University, Abu Dhabi, 6 MetroTech Center, Brooklyn, NY 11201; [4]RWTH Aachen University, Mies-van-der-Rohe-Straße 1, 52074 Aachen, Germany; [5]Alps-Adriatic University Klagenfurt, Lakeside park Gebäude B04a, 9020 Klagenfurt, Austria; [6]Department of Mechanical Engineering, Macdonald Engineering Bui, Sherbrooke Street West, H3A 2K6 Montreal, Quebec, Canada; [7]Purdue University, School of Mechanical Engineering, Weldon School of Biomedical Engineering, West Lafayette, IN 47907; [8]Graduate School of Information Science, Japan Advanced Institute of Science and Technology, Nomi-city, Ishikawa 923-1292, Japan

Abstract: Acoustic data has long been harvested in fundamental voice investigations since it is easily obtained using a microphone. However, acoustic signals alone do not reveal much about the complex interplay between sound waves, structural surface waves, mechanical vibrations, and fluid flow involved in phonation. Available high speed imaging techniques have over the past ten years provided a wealth of information about the mechanical deformation of the superior surface of the larynx during phonation. Time-resolved images of the inner structure of the deformable soft tissues are not yet feasible because of low temporal resolution (MRI and ultrasound) and x-ray dose-related hazards (CT and standard x-ray). One possible approach to circumvent these challenges is to use mathematical models that reproduce observable behavior such as phonation frequency, closed quotient, onset pressure, jitter, shimmer, radiated sound pressure, and airflow. Mathematical models of phonation range in complexity from systems with relatively small degrees of freedom (multi-mass models) to models based on partial differential equations (PDEs) mostly solved by finite element (FE) methods resulting in millions of degrees-of-freedom.

We will provide an overview about the current state of mathematical models for the human phonation process, since they have served as valuable tools for providing insight into the basic mechanisms of phonation and may eventually be of sufficient detail and accuracy to allow surgical planning, diagnostics, and rehabilitation evaluations on an individual basis. Furthermore, we will also critically discuss these models w.r.t. the used geometry, boundary conditions, material properties, their verification, and reproducibility.

Keywords: Human phonation, multi-mass models, models based on partial differential equations.

1. INTRODUCTION

The human phonation process is a complex interaction between the flow through the larynx, the vibrating vocal folds and the generated sound. By compression of the lungs air flow is generated which flows through the glottis being located inside the trachea. Air flow is a major mechanism of energy transport between exhaling air and vocal fold motion inside the larynx. When physiologic and geometric conditions are right, self-oscillation of the vocal folds initiates a pulsating air flow. Fig. (**1**) shows a frontal cut through the larynx displaying in Fig. (**1a**) the anatomical components and illustrating in Fig. (**1b**) the sound sources that exist in phonation. Basically, we differentiate between three sources: the volume-induced sound (mono-pol sources) due to the modulated flow resulting from the self-sustained oscillation of the vocal folds, the eddy-induced sound (quadrupole sources) which emerges from turbulent flow structures, and the sound from the vibrating vocal folds (dipole sources).

Empirical studies of laryngeal flows have often been used to estimate pressure and velocity distributions within the glottis. However, due to space limitation of the larynx, the measurable variables are quite limited and many important flow phenomena are difficult to obtain. One alternative is to use the numerical simulations that provide more detailed information about the flow field and pressure distributions. The complexity of the problem restricts computational simulation approaches. One classical and very popular approach to the study of voice production is to construct a multi-mass model of the vocal fold vibrations. Depending upon the number of masses, the model may represent simple low-dimensional self-sustained oscillations

*Address correspondence to this author at the Applied Mechatronics, Alps-Adriatic University Klagenfurt, Lakesidepark Gebäude B04a, 9020 Klagenfurt, Austria; Tel: +43 (0)463 2700 3563;
Fax: +43 (0)463 2700 3698; E-mail: stefan.zoerner@uni-klu.ac.at

1574-8936/11 $58.00+.00

A

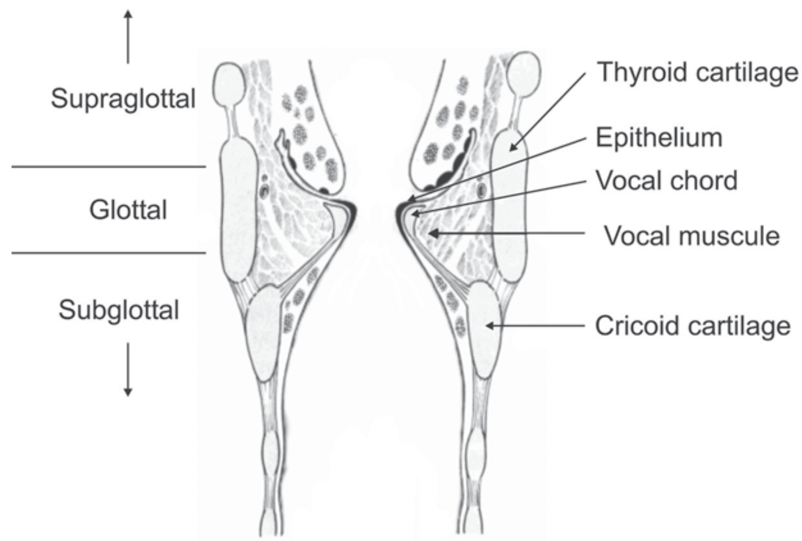

B

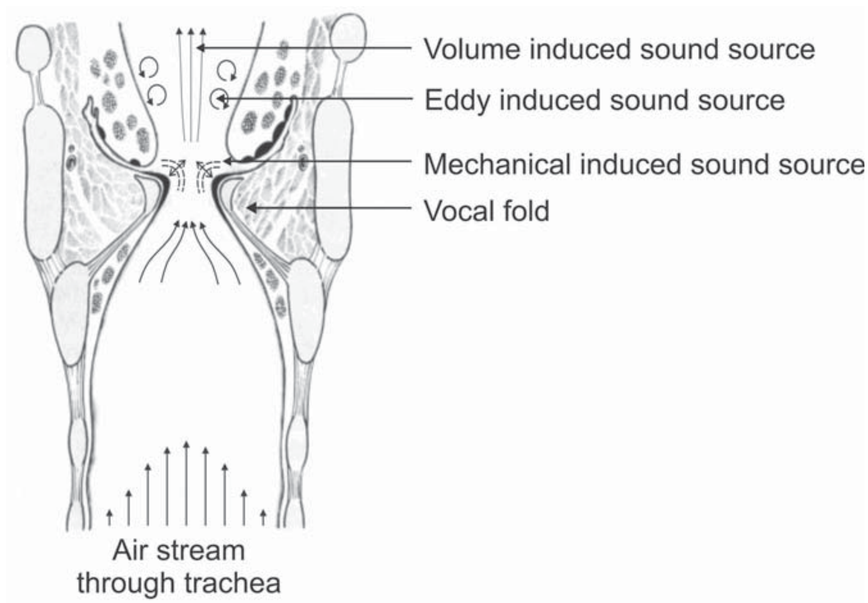

Fig. (1). Frontal cut through the larynx showing the anatomical constitution and the different sound sources. (**a**) [One-mass model of Flanagan and Landgraf (1968).]. (**b**) [Two-mass model of Ishizaka and Flanagan (1972).]. (**c**) [Three-mass model of Story and Titze (1995).]. (**d**) [$L \times M \times N$ point mass model of Titze (1973, 1974).]

of the vocal folds (see, e.g., [1]) or more complex vibrations with many oscillatory modes (see, e.g., [2-4]). The second approach consists in models based on the underlying partial differential equations (PDEs) of the flow, the structural vibrations of the vocal folds and the acoustic field. Due to limitations in computer resources, full coupling between all three fields for realistic geometries is currently not feasible. This review will present various models and their solution methods (see, e.g., [5-10]).

The aim of the review article is to provide an overview of mathematical models and their applications. Therewith, we will describe the different models used in Sec. 2 and in Sec. 3 the results of these approaches. Finally, we will provide a discussion about the models with respect to the used geometry, boundary conditions, material properties, their verification, and reproducibility.

2. MATHEMATICAL MODELS OF HUMAN PHONATION

2.1. Multi-Mass Models

The key idea of the multi-mass model is to divide the vocal fold tissue into small portions of masses and then couple the neighboring masses via springs. Flanagan and Landgraf [1] modeled the vocal fold vibrations with a single mass-spring oscillator driven by airflow from the lungs (see Fig. **2a**). The model produced self-sustained oscillations under the condition that the acoustic impedance of the vocal tract is inertive. Because of its single degree of freedom, this model does not produce the vertical phase difference needed for efficient flow-induced oscillation. Ishizaka and Flanagan [11] introduced a two-mass model that simulates the core mechanism of the vocal fold vibrations such as the phase shift of lower and upper edges of the vocal folds introduced by Stevens [12] (see Fig. **2b**). The resulting wave-like motion allows an efficient energy transfer from the airflow to the vibrating vocal folds [13], enabling self-sustained oscillations with or without the vocal tract. This model has been widely used as a simple reduced order model of the vocal folds. Asymmetry between the right and left vocal folds was later introduced by Ishizaka and Isshiki [14] into the two-mass model to study various pathologies. Steineke and Herzel [15] simplified the asymmetric two-mass model of Ishizaka and Isshiki to study nonlinear dynamics and bifurcations of the vocal fold model. Döllinger *et al.* [16] developed a method to estimate the parameter values of the Steineke-Herzel model that may correspond to endoscopic image series of the vocal folds. Despite its simplicity and efficiency, the weakness of the two-mass model is its lack of direct physiological correlation between the spring stiffness and the effects of muscle contraction. To better link the model to physiology, Story and Titze [17] introduced a three-mass model close based on the body-cover theory of Hirano [18,19]. Parameter values may be in close correspondence to physiological measurements. Titze and Story [20] further developed rules for controlling the parameters of the three-mass model according to muscle activity, which successfully reproduce Hirano's four baseline phonations cases [18]. Adachi and Yu [21] introduced a one-mass model that can vibrate both parallel and perpendicular to the airflow and applied it to soprano singing. The idea of a smooth borderline between the edges of the vocal fold was introduced by Childers [22] to a one-mass model, which simulates voice pathologies as well as vocal fry. Lous *et al.* [23] also utilized a smooth geometry in the two-mass model, and applied it to prosthesis design.

Another important approach to the multi-mass modeling of the vocal folds has been provided by the mucosal wave model [13]. This model assumes small-amplitude oscillations of the vocal folds and represents the oscillatory motion as a surface wave propagating in the direction of the airflow. The dynamics are described only in terms of the displacement of the midpoint position of the vocal fold and its velocity. This simplification enables analytical treatment for understanding the basic principles of the vocal folds dynamics. Although the small-amplitude restriction means that the model applies only to oscillations with slightly abducted vocal folds without glottal closure, the model is valid for falsetto and breathy voice and has been shown to be useful for establishing the oscillation threshold condition [13]. The model has been updated and extensively used in analytical studies [24-27] as well as in full simulations of the vocal folds [28,29].

The multi-mass models with limited degrees of freedom such as one-mass, two-mass, and three-mass models are reduced order models of the vocal folds. Extensions of the simple models to more complex models have also been made. Titze [2,30] represented both the vertical and longitudinal modes of vocal fold vibrations with a sixteen-mass model. This model consisted of eight coupled longitudinal sections, each with two masses in the coronal plane. The two-masses in each longitudinal section had a vertical degree of freedom which simulated two-dimensional trajectories of the vocal fold. Waves in the longitudinal dimension may be also generated. Koizumi *et al.* [3] described several variations of the simple two-mass model with longitudinal discretization to synthesize more natural sound. Wong *et al.* [31] combined the two-mass approach with longitudinal discretization and created a ten-mass model to study voice pathologies. Kob [4] modified the sixteen-mass model [2] to simulate various singing voices. A general formula for a $L \times M \times N$ point mass model has been described by Titze [32], where L is the number of masses in the medio-lateral direction, M is the number of masses in the anterior-posterior direction, and N is the number of masses in the inferior-superior direction (see Fig. **2d**).

Reduced order models capture the essence of the vibration mechanisms, which is hidden in the complex oscillation of the vocal folds. Since the number of model parameters is limited, low-dimensional model results have a weak dependence on parameter selection. Low-dimensional models are also appropriate to study the nonlinear dynamics [33] of vocal fold vibrations. Reduced order models are of course limited in geometrical details and the number of oscillatory modes which are present in the real vocal folds. In contrast to low-dimensional models, the advantage of the complex high-dimensional models is that they describe anatomical and physiological structures of the real vocal folds in detail. They produce the main oscillatory modes and also many other complicated spatial-temporal modes, which exist in real vocal folds. Such detailed models involves many parameters, whose values are still not precisely known.

To describe the flow inside the glottis, a simple mathematical model is usually preferred in multi-mass modeling. Assuming a quasi-steady and incompressible flow, Bernoulli's equation is widely applied. For the computation of the pressure distribution within the glottis, a prior computation of the location of the flow-separation is crucial. In particular, during the closing phase of the phonatory cycle, the glottal walls take a diverging shape that creates a flow-separation somewhere along the diverging walls. Position of the flow-separation point has a strong influence on the vocal folds oscillation, because it determines not only the volume flow velocity but also the aerodynamic force acting on the vocal fold tissues. The flow-separation was also found to have a positive effect on the lowering of the phonation threshold pressure, making it easier to create self-oscillation of the vocal folds [34]. In Ishizaka and Flanagan's model (1997), flow-separation was located at vocal fold edges that are fixed in space. Then, Pelorson *et al.* [35] introduced a model of moving flow-separation point based on a boundary-layer theory and applied it to a two-mass model. Introduction of the flow model to compute the moving separation point made the simulated signal quite similar to the real glottal signal. Later,

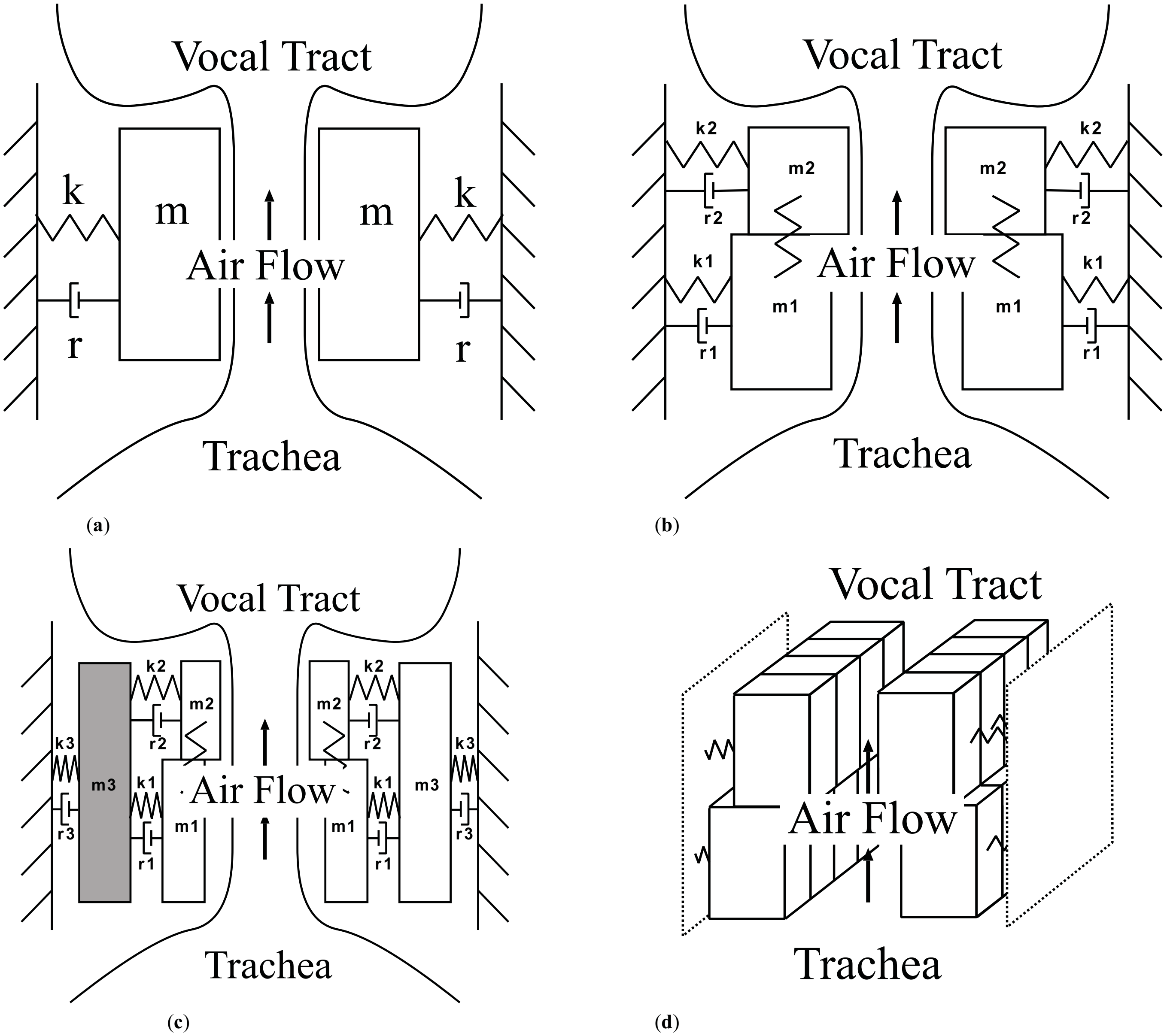

Fig. (2). Schematic illustration of different multi-mass models.

simplified technique for computing the moving flow-separation point based on a geometric criterion has been also developed [23]. Here the flow-separation is located at a point, where the glottal area is related to the minimal glottal area with a constant ratio, referred to as separation constant. Although some discrepancy can be created between the precise flow model and the simplified geometric model, the geometric models are nonetheless found to be quite useful for realistic simulation of the vocal folds and therefore widely used [23,36].

A more sophisticated approach is presented by Tao and Jiang [37], which combine the Navier-Stokes equations and a two-mass model for the vocal folds and compare this to a Bernoulli based approach.

2.2. PDE Based Models

The partial differential equation (PDE) based modeling approach is aimed at resolving all physical details of the phonation process in space and time. Therewith, the PDEs of the flow, structural mechanics and acoustic fields with all their relevant interactions have to be solved. As displayed in Fig. (**3**) fluid forces act thereby on the neighboring vocal folds, which are deformed and thereby influence the velocity of the adhering fluid particles. Due to the solid deformation, the fluid domain changes and has to be adapted. The fluid-acoustics interactions are described by aeroacoustics (flow induced sound) and the solid-acoustics coupling by claiming coincident surface velocity (acceleration). However, due to the enormous complexity, current PDE based approaches use many simplifications. For most PDE based models, the finite element (FE) method has been used to numerically solve the arising PDEs, including their couplings.

A first continuum mechanical model was described by Alipour *et al.* [5] using the FE method for the computation of the vocal fold vibrations. In their 2D model the mechanical field was discretized with finite elements and the fluid forces

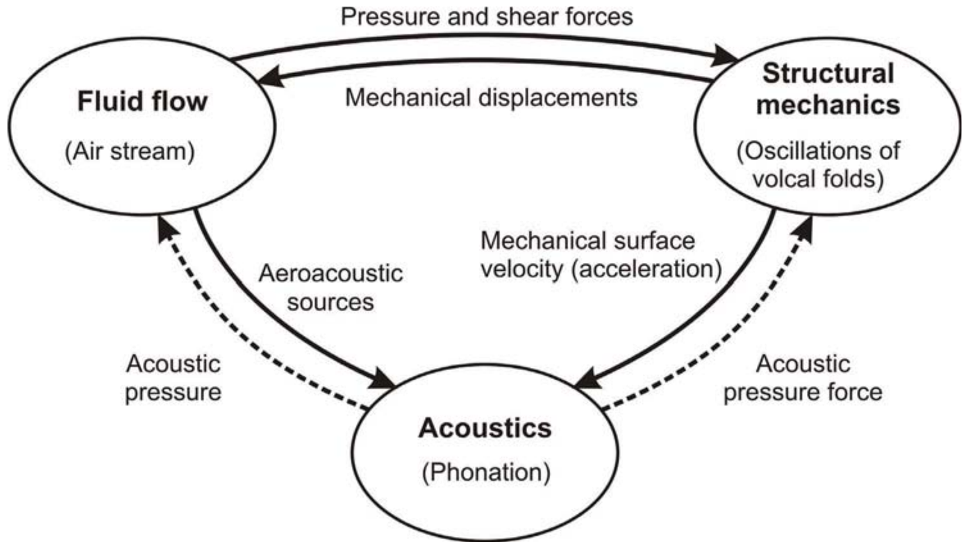

Fig. (3). Fluid-Solid-Acoustic interactions.

were modeled based on Bernoulli's equation. A comparison between a Bernoulli and a 2D Navier-Stokes solver was discussed by Vries *et al.* [38] with a hemilarynx model (i.e. half larynx). For a pure flow field simulation in the larynx, several numerical models are available, e.g. [39-41]. Thomson *et al.* [42] used a hemilarynx continuum mechanical model to clarify the causes for self-sustained vocal fold oscillations. They confirmed that a cyclic variation of the glottis profile from a convergent to a divergent shape is a key factor for self-sustained vocal fold oscillations. Tao *et al.* [6] applied a collision model with fluid-solid interaction within a strongly coupled fluid-solid algorithm to treat the interactions. Fully three dimensional (3D) coupled simulations to analyze human phonation are very challenging for current computing resources. A 3D fluid-solid coupled model based on the FE method was done by Rosa *et al.* [7]. The authors clearly demonstrate the self-sustained vocal fold oscillations, although the grid for the flow computation was quite coarse. The first fluid-solid interaction model with fully resolved flow computation was done by Luo *et al.* [43]. They used a realistic 2D setup and applied the immersed boundary (IB) method for fluid-solid interaction. Their results are quite similar to the one presented by Link *et al.* [10], especially in that they were also able to obtain the so-called Coanda effect ([44,45]). Therewith, the jet shows significant asymmetry and attaches stochastically to either side of the pharynx wall. This phenomenon is caused by a minor asymmetry of the jet in the geometrical configuration which induces a pressure field leading to a curvature of the jet. The curved streamlines strengthen the pressure gradient normal to the mean flow direction. Thus any initial disturbance is reinforced forcing the jet to attach to the curved wall.

Beside the fluid-solid interaction, the computation of flow-induced sound is a second main challenge. Aeroacoustic sound generation mechanisms have been investigated by Zhao *et al.* and Zhang *et al.* [8,46,47]. They described the aerodynamic generation of sound in a rigid pipe under forced vibration. The fluid-solid interaction was neglected and they focused on fluid-acoustic coupling based on Lighthill's acoustic analogy, which was solved with an integral method---the so-called Ffowcs Williams-Hawkins (FWH) method [48]. The results based on the FWH method were in good agreement with results based on direct numerical simulations, which solves the compressible Navier-Stokes equations. Further investigation have been presented by Suh *et al.* [49]. Complementary to these studies, a theoretical approach was proposed by Krane [50]. The acoustic source model was based on a prescribed jet profile using a train of vortex rings and applied to an axisymmetric model of the vocal tract. Bae and Moon [9] applied a 2D axisymmetric model studying the flow and the acoustics in the vocal tract with glottal motion. A hybrid method was applied, describing the flow field via the incompressible Navier-Stokes equations and computing the acoustic field with the perturbed compressible equations. Gloerfelt and Lafon [51] investigate the flow and the acoustic field in a 3D slit-like constricted channel with a DNS model. The channel geometry corresponded to a simplified and up-scaled glottal constriction during phonation. A fully coupled simulation scheme taking into account the interaction between all three physical fields restricted to 2D geometries was done by [10].

A major problem of PDE based models, which is currently not fully solved, is to take contact between the vocal folds into account. One of the first structural models including contact used a setup of one vocal fold [5]. Therewith, each FE node of the surface of the vocal fold, which reaches the symmetry plane, looses one degree of freedom. Horáček *et al.* [52,53] used a low degree-of-freedom model for the simulation of vocal fold oscillation. Contact was implemented using a Hertz formulation. In their study they calculated the maximum collision stress versus prephonatory glottal gap width and lung pressure. They obtained values around $2-3\,\mathrm{kPa}$. Rosa *et al.* and Tao *et al.* [6,7] applied a full flow-structural mechanical model. Both used a similar approach: When contact is detected, a force is computed which prevents the concerning nodes from interpenetration. Tao *et al.* [6] used the more extensive Augmented Lagrangian method as contact algorithm in their self-oscillating 3D half model. The major problem in fluid-solid interaction computations using volume discretization methods (such as the finite-volume or finite-element method) is that the structural side has to ensure that there are no zero-volume (3D) or zero-area (2D) elements. This is achieved by enforcing a minimum gap between the vocal folds by contact formulations. Decker *et al.* [54] defined a minimal glottal gap of $0.048\,\mathrm{mm}$ in a 2D half-model. A rigid target line is defined external from the vocal fold. Luo *et al.* [43] ensured a gap of $0.2\,\mathrm{mm}$ by a kinematic constraint in a 2D model, which uses the immersed boundary (IB) method. In Zheng *et al.* [55] a sharp-interface immersed boundary method flow solver is coupled to a finite-element method solid dynamics solver for 2D and 3D problems. Furthermore, a penalty coefficient method introduced by Belytschko [56] is implemented to model vocal fold contact. With a fixed pressure at the inlet of $1\,\mathrm{kPa}$, $0\,\mathrm{kPa}$ at the outlet and an additional zero gradient normal velocity at both openings, results show a vibration frequency of $242\,\mathrm{Hz}$ which can also be seen in the flow spectrum analyses. Based on this method Seo *et al.* [57] implemented the acoustics in 2D and the sound propagation included the vocal tract and the region around the speaker. With a given fluctuating inlet flow rate they were able to simulate a monopole sound source around the mouth and the propagation into the surrounding region.

3. SIMULATION RESULTS FROM DIFFERENT MODEL APPROACHES

3.1. Three-Mass Model

As an example of low-dimensional multi-mass model, a three-mass model by Tokuda *et al.* [53] is considered in this subsection. This model was constructed to replicate as closely as possible the sudden chestfalsettotransitions and accompanying voice instabilities, which were observed in experiments with excised human larynges. Registers are one of the most important voice qualities for classifying the type of phonations and the transition between them is essential in the singing voice. The careful study of van den Berg *et al.* [54, 55] simulated chest and falsetto registers in excised human larynx experiments, which has been recently repeated by Horáčček *et al.* [56]. The three-mass model was designed to capture the gross features of this experiment.

The three-mass model was constructed by adding one additional mass to the two-mass model [11] as shown in Fig. (**4a**); note that the present three-mass configuration is different from that of Story and Titze [17], who implemented the body-cover structure in Fig. **2b**). The three masses are suitable for representing these coexistent vibratory patterns, which may correspond to chest and falsetto registers [53]. The main modeling assumptions are (1) the three masses are coupled by linear springs, (2) the air flow inside the glottis is described by Bernoulli's principle below the narrowest part of the glottis [15], (3) there is no influence of the vocal tract and the subglottal resonances (as in the experiment), and (4) the left and the right vocal folds are symmetric with respect to each other. The model equations are

Equation 1-3:

$$
\begin{aligned}
m_1\ddot{x}_1 + r_1\dot{x}_1 + k_1x_1 + \Theta(-a_1)c_1\left(\frac{a_1}{2l}\right) + k_{1,2}(x_1-x_2) &= ld_1P_1\\
m_2\ddot{x}_2 + r_2\dot{x}_2 + k_2x_2 + \Theta(-a_2)c_2\left(\frac{a_2}{2l}\right) + k_{1,2}(x_2-x_1) &= ld_2P_2\\
m_3\ddot{x}_3 + r_3\dot{x}_3 + k_3x_3 + \Theta(-a_3)c_3\left(\frac{a_3}{2l}\right) + k_{2,3}(x_3-x_2) &= ld_3P\_3
\end{aligned}
$$

The dynamical variables xi represent the displacements of the masses mi (lower mass: i = 1, middle mass: i = 2, upper mass: i = 3), where the corresponding glottal areas are given by $a_i = a_{0i} + 2lx_i$ (a_0i: prephonatory area, l: length of the glottis). The constant parameters r_i, k_i, d_i represent damping, stiffness, and thickness of the masses mi, respectively, whereas $k_{i,j}$ represents the coupling strength between the two masses mi and mj . The effect of collision between the right and left vocal folds is simply described as an additional stiffness c_i, which is to force the vocal folds apart from each other (more precise modeling of the collision impact is discussed, e.g., in [50]). The additional stiffness c_i is activated only when the corresponding glottal area a_i takes a negative value, where the collision function is given by $\Theta(x) = 0\,(x \leq 0)$; $\Theta(x) = 1\,(0 < x)$. The pressures p_i, which act on the masses m_i, and the glottal volume flowvelocity U obey Bernoulli's equation below the flow-separation point, which is defined as the narrowest part of the glottis [15]. Bernoulli's equation is

$$
p_s = p_1 + \frac{\rho}{2}\left(\frac{U}{a_1}\right)^2 = p_2 + \frac{\rho}{2}\left(\frac{U}{a_2}\right)^2 = p_0 + \frac{\rho}{2}\left(\frac{U}{a_{\min}}\right)^2
$$

where ρ represents the air density ($\rho = 1.13\,\mathrm{kg/m^3}$), p_s is the subglottal pressure, and p_0 is the supraglottalpressure. The narrowest area of the glottis is given by $a_{\min} = \min(a_1, a_2, a_3)$. By setting $p_0 = 0$, the pressures and the flow are obtained as

$$
\begin{aligned}
p_1 &= p_s[1-\Theta(a_{\min})\left(\frac{a_{\min}}{a_1}\right)^2]\Theta(a_1)\\
p_2 &= p_s[1-\Theta(a_{\min})\left(\frac{a_{\min}}{a_2}\right)^2]\Theta(a_1)\Theta(a_2)\Theta(a_1-a_3)\Theta(a_2-a_3)\\
p_3 &= 0\\
U &= \sqrt{\frac{2p_s}{\rho}}a_{\min}\Theta(a_{\min})
\end{aligned}
$$

To simulate the excised larynx experiment, a tension parameter $\tilde{Q}$ is controlled, where $\tilde{Q}$ determines the size and the stiffness of the second mass in a way that it linearly controls the frequency of the second mass. The other parameter values were adopted from the standard values established in the two-mass models[11, 15]. To integrate the three-mass model equations (1)-(3), a fourth-order Runge-Kutta method was used.

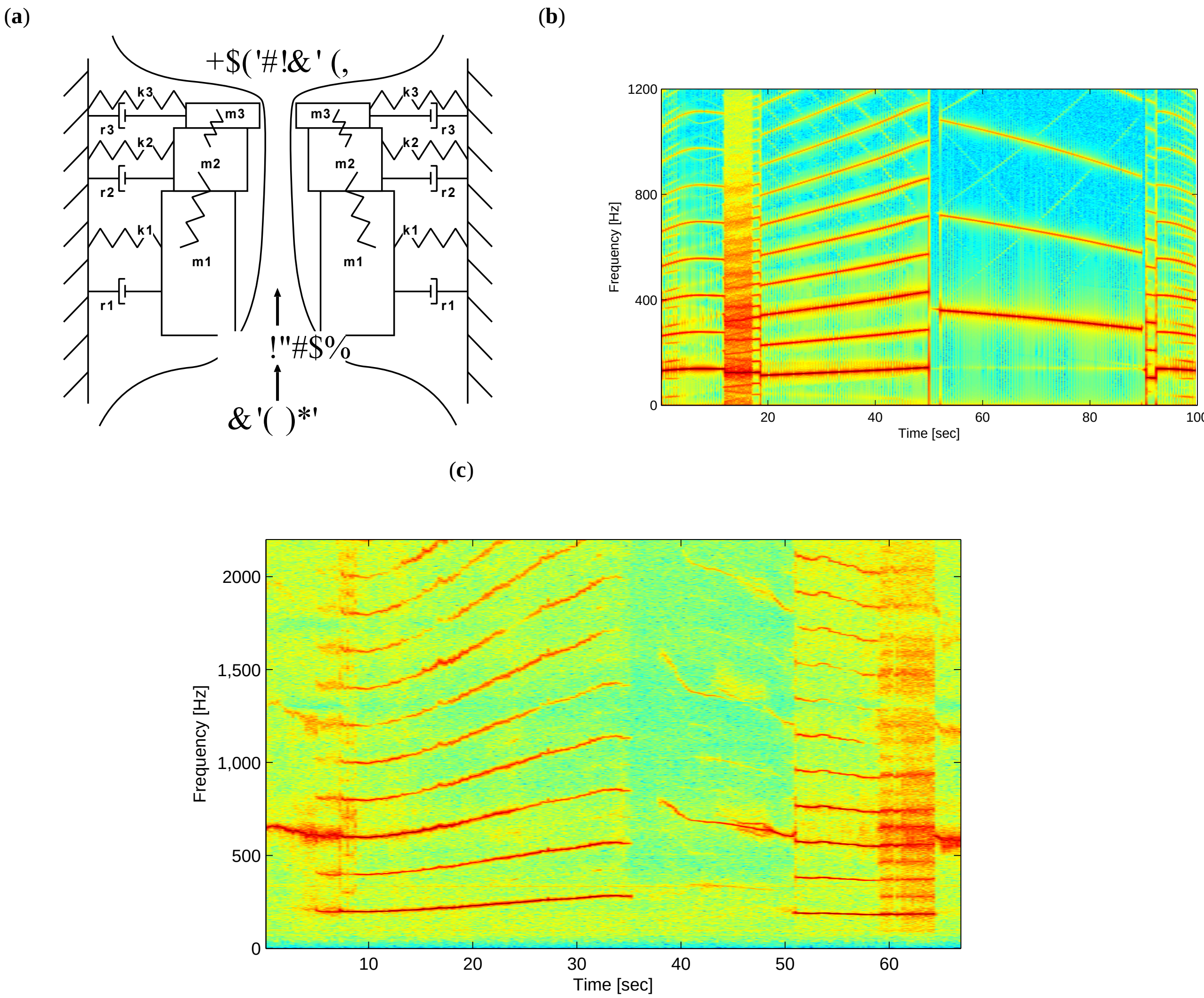

Fig. (4). (**a**) Schematic illustration of the three-mass model. The left and right vocal folds have a symmetric configuration. Each vocal fold is composed of three masses coupled by linear springs. (**b**) Spectrogram of the output signal from the three-mass model. The tension parameter is increased from $\tilde{Q}=0.9$ to $\tilde{Q}=1.58$ in $t\in[0,50]$ and then decreased back to $\tilde{Q}=0.9$ in $t\in[50,100]$. (**c**) Spectrogram of the microphone signal recorded from an excised human larynx by Horáček *et al.* [61]. Longitudinal tension of the vocal folds, monitored by force transducer, was smoothly increased or decreased by rotating the thyroid cartilage.

Fig. (**4b**) shows a spectrogram of the three-mass model by increasing the tension parameter $\tilde{Q}$ from t = 0 s to t = 50 s and then by decreasing it from t = 50 s to t = 100 s. This resembles the spectrogram of Fig. (**4c**), which represents the real experiments with excised human larynx when the vocal folds were symmetrically elongated and shortened. In the direction of increasing $\tilde{Q}$, low-frequency oscillations-dominate the spectrogram, whereas in the direction of decreasing $\tilde{Q}$ higher-frequency oscillations last until they switch to low-frequency oscillations at t = 90 s. This hysteresis is due to the coexistence of the low-frequency and high-frequency oscillations, which correspond respectively to chest and falsetto registers according to the vibratory patterns observed in the simulation. Namely, a complete glottal closure was observed for the chest-like vibrations, whereas glottal area was not completely closed for the falsetto-like vibrations (no figure shown). Irregular dynamics are observed around t = 15 s, whereas short interruption of phonation ("aphonic episode") exists at t = 50 s. These instabilities are also found in the experiment. The simulations therefore reveal that a simple three-mass model can reproduce many of the complex transitions observed experimentally. Since the three-mass model represents just the core mechanisms of the vocal folds oscillations, gross features of the register transitions simulated by the present model are expected to be found commonly in other vocal fold models.

3.2. 3D Flow and Acoustic Simulations

Based on Lighthill's acoustic analogy a 3D model was developed to compute the flow induced sound within the larynx. Therewith, the incompressible form of the Navier-Stokes equations was discretized and numerically solved by the finite-volume (FV) method in a cell-centered formulation on a fully block structured grid with the open source computational fluid dynamics (CFD) code OpenFOAM [57]. To fully resolve the flow about 1 million FV cells were used for the spatial discretization. In a second step, Lighthill's stress tensor was evaluated from the results of the flow field simulation [58] and the acoustic field was computed by numerically solving the inhomogeneous wave equation by the FE method on the same computational grid using CFS++ [59].

The computational setup consists of a rectangular channel with elliptic shaped constriction as sketched in Fig. (**5**) (for details of the experimental setup, see [60]). Under the precondition that Reynolds, Strouhal and Euler number are conserved as given in Table **1** the CFD and CAA computations are coupled by the hybrid approach used by Mattheus *et al.* [61]. The CFD model has been validated with the experimental results of Triep *et al.* [60] and by Schwarze *et al.* [62]. The elliptic constriction reduces the area of the transversal cross-section by a factor of 18 that equals an area blockage of nearly 95%. In the coronal cross section, the constriction is contoured like a nozzle with a smooth convergent entry and a strong divergent exit. As inlet velocity a characteristic wave form as shown in Fig. (**6**) has been taken. The resulting flow divided up in the three velocity components $U_{\mathrm{x}}, U_{\mathrm{y}}, U_{\mathrm{z}}$ at probe point P0 (1D,0,0), which is located one channel width D downstream from glottal constriction, are plotted in Fig. (**7**). The waveforms are recovered in the streamwise velocity component U_{x}.

Additionally, the fluctuations of all velocity components indicate the effects of the induced vortices in the flow. The corresponding normalized frequency spectra of the time series at probe point P0 are displayed in Fig. (**8**). In all spectra, a peak with strongest intensity is observed at the base frequency f_0 of the prescribed volume flow waveforms. To be pointed out, are the significant larger values of intensity for frequencies with a factor between 30 and 40 times higher than the base frequency. They are generated in the jet shear layer and transported downstream until they decay into smaller structures. The acoustic signals obtained from the aeroacoutsic simulations based on Lighthill's acoustic analogy are provided in Fig. (**9**). For all setups,the base frequency of the inflow velocity (135 Hz) is recovered in the spectra of the acoustic sound pressure level (SPL) and their harmonics with lower amplitudes. For the glottal waveform, the spectra of the SPL includes a broadband sound at $f/f_0 \simeq 30-40$. From the inspection of the SPL spectra at different locationsin the supraglottal region, it is found that the stochastically generated sound varies in space with the highest amplitude at probe point P0. At this point the flow is quite turbulent compared to the point at outflow or at the glottis. With respect to the results of the investigations by Bae and Moon [9] and Gloerfelt and Lafon [49] for similar flow configurations, our spectra have similar slopes in both the lower (dominated by the base frequency at its harmonics) and the higher frequency part, where the broadband sound is found. Therefore, we conclude that the hybrid model approach is well suited to resolve the main features of the flow and the acoustic spectra in the laryngeal channel.

3.3. 2D Fluid-Structure Simulations

This section describes results of simulated pulsatile flow in a model larynx that is shown in Fig. (**10**) by fully taking the flow-structural mechanics interaction into account. The channel height was 2.5 cm with 5 cm inlet duct and 50 cm outlet duct. The vocal fold model had equilibrium height of 1:15 cm with amplitudes ranging from 0 to 0.9 mm. A symmetric flow condition was assumed and only lower half of the channel was discretized. The computational grid was divided into three blocks. Block 1 (inlet) had 21×46 grid point, block 2 (glottis) had 31×26 grid points, and block 3 (outlet) had 31×26 grid points. Results were obtained for various control parameters such as Reynolds number, frequency, amplitudes and phase lead of inferior-superior heights. For the continuum model of vocal fold vibrations, a few assumptions are stated that help to simplify the job

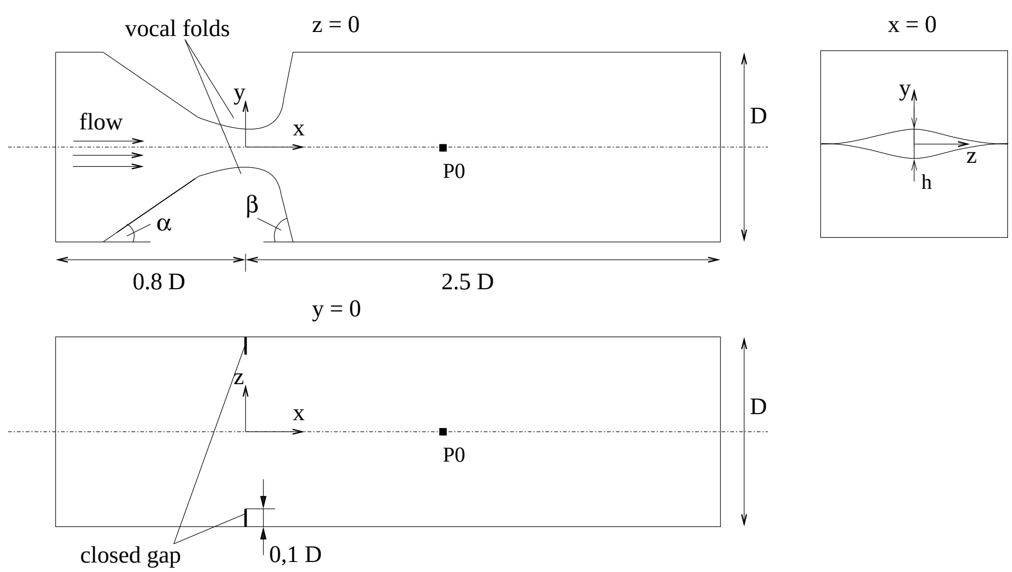

Fig. (5). Sketch of the 3D computational domain, coronal (xy) (upper left), sagittal (xz) (lower) and transversal (yz) (upper right) cross sections, channel width D = 60mm, max. opening of the constriction h = 8mm, contour angles α = 45° and β = 80°.

Table 1. Characteristic Values, Similarity Parameters and Scaling Factors Between Air Flow and Up-Scaled Water Flow in the Laryngeal Channel

Characteristic Value for Glottal Airflow	Resulting Similarity Parameters
$U_m = 30\, ^m/_s$	$Ma = 0.1$
$h = 2mm$	$Re_m = 5000$
$f_0 = 135Hz$	$Sr = 0.01$
$\Delta p = 1400Pa$	$Eu = 1$

without sacrificing the accuracy:

- The vibration causes small deformations (linear elasticity).
- The vibration takes place in a single plane only.
- The tissue layers of the vocal fold are either isotropic or transversally isotropic (with the plane of isotropy being perpendicular to the tissue fibers). This assumption is based on measured mechanical properties of the vocal fold tissues.
- The effect of grids motion during finite element space integration is neglected, assuming fixed control volume for integration.

Fig. (**11**) shows one cycle of the mean velocities (cross-sectional average) at the glottal inlet (U_{im}) and the glottal outlet (U_{om}). The phase was varied from -60 to 90 degrees while other parameters were held constant (Reynolds number Re $= 1000$, frequency $f_0 = 100$ Hz, and amplitudes $A_{\mathrm{i}} = 0.75$ mm, $A_{\mathrm{s}} = 0.90$ mm). There is a reverse flow in a portion of each cycle at the inlet and outlet sections. This is due to the displacement flow caused by the wall motion. The phase difference plays an important role in the flow and motion interaction. Since this is a forced oscillation model, phase changes of the wall motion could have a positive or negative effects on the airflow. At positive phase values a large reverse flow will appear at the glottal exit near the end of the cycle. The effects of phase difference on the transglottal pressure (tgp) are shown in the Fig. (**11c**). There is a positive pressure gradient in the direction of flow for positive phase values during closing portion of the cycle. The experimental data on the excised larynx shows this phase is between 60–90 degrees. A phase value of 60 is used for the remaining study

3.4. 2D Fluid-Structure Simulations with Contact

The contact formulation, which is used, is an augmented Lagrangian method similar to the model of Luo *et al*. [41]. It is based on an algorithm, which was published by Simo and Laursen [63]. In this algorithm, a standard penalty method is iteratively extended by a distance function until a Lagrange multiplier is found which prevents interpenetration of the corresponding nodes.

The weak formulation for structural mechanics is extended by an augmented penalty regularization term, which reads as follows

$$\int_{\Gamma_c} < \lambda_N^{(k)} + \epsilon_n g(x) > (\delta x) \cdot n(x) d\Gamma \,.$$

In (9) Γ_c denotes the contact surface, $\lambda_N^{(k)}$ the Lagrange multiplier, ϵ_n the penalty parameter, and $g(x)$ a function, which determines the closest projection of a point onto an admissible region and the outward normal of the current configuration $n(x)$.

In (9), $< \lambda_N^{(k)} + \epsilon_n g(x) >$ is regarded as current estimate of the correct Lagrange multiplier. The correct multiplier is found iteratively by updating $\lambda_N^{(k+1)} =< \lambda_N^{(k)} + \epsilon_n g(x) >$ until g(x) becomes smaller than a prescribed tolerance. The advantage of this method is the better conditioning of the equations compared with the earlier penalty methods. The cost of the method is the use of an additional variable (λ_N). Corresponding to the impact forces, which are transferred between the vocal folds during glottal closure, the flow has to be stopped. A straight-forward way to approximate the flow effects in finite-volume models, where zero-volumes are not possible, is introducing an artificial momentum source when the vocal folds are nearly closed. This (artificial) momentum source SM, which is added to the Navier-Stokes equations, is calculated according to

$$S_{\mathrm{M},i} \;=\; -\,\frac{1}{2} K_1 \,\rho\, |v|\, v_i$$

with the loss coefficient Kl, the absolute velocity of the fluid $|v|$, and the velocity v_i in direction i. K_1 is dependent of the distance between the vocal folds d_{VF}

$$K_1 \;=\; \begin{cases} 0 & \text{for } d_{\mathrm{VF}} \geq d_{\mathrm{thr}} \\ \chi & \text{for } d_{\mathrm{VF}} < d_{\mathrm{thr}} \end{cases}$$

In (11) d_{thr} is the threshold value for closure, and χ an arbitrary value with the unit of [kgm^4]. The effects of contact are shown on two setups. The first setup just includes the structural contact while the second additionally comprehends the arbitrary loss coefficient for stopping the flow in the glottal gap. The model setup on the structural side includes two contact pairs. Each of them consist of a contact and target area whose normal directions tend toward each other (Fig. (**12**), left-hand side). Both of the target areas are located in the glottal gap and form a permanently open channel of 0.1mm. This approach ensures that the mesh in the flow model is not distorted to zero or negative volumes.

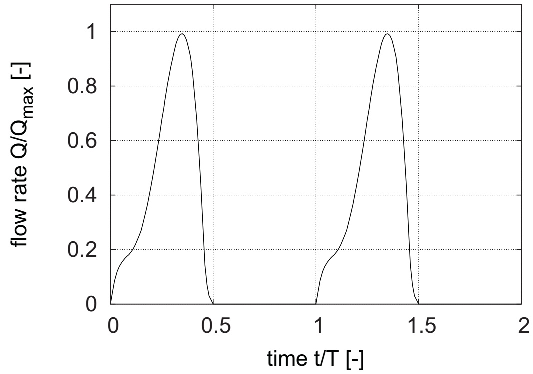

Fig. (6). Prescribed volume flow waveform at the inlet as a characteristic waveforms for glottal cycle. Flow rate on the y-axis is normalized to its maximum values Q_{max} of one cycle, max value is $U_{glottal}^{in,max} = 0.129\text{m/s}$.

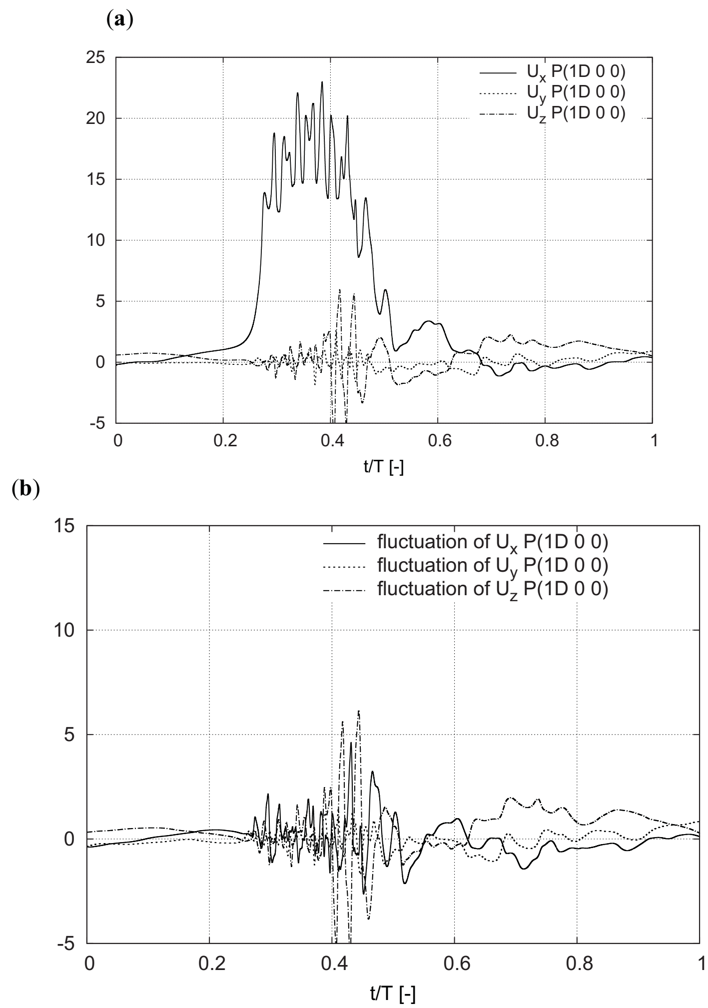

Fig. (7). Time-series of velocity components U_x (solid line), U_y (dotted line) and U_z (dash-dot line) and their fluctuations U'_x (solid line) , U'_y (dotted line) and U'_z (dash-dot line) relative to phase averaged velocity. $\bar{U}_{phase}$ at probe point P0 (1 D,0,0), located one channel width D downstream from constriction on the central axis. The velocities are normalized to the maximum velocity of the inflow boundary condition in Fig. (**6**).

The closure effects on the fluid side are introduced by an artificial momentum source. The volume in which the loss coefficient is introduced is shown in Fig. (**12**) (right-hand side, denoted as "glottal region").When the vocal folds distance falls below the threshold distance d_{thr} of 0.1 mm, χ takes the value of $10^8\ \mathrm{kgm}^4$ (see (10)).

A full flow-structural mechanical interaction simulation of both setups (with and without the artificial loss) has been carried out with a total simulation time of 90 ms. It can be seen that both of the closure approaches influence each other. When the loss coefficient is used, less structural contact takes place Fig. (**13a**,**b**). That means that already the

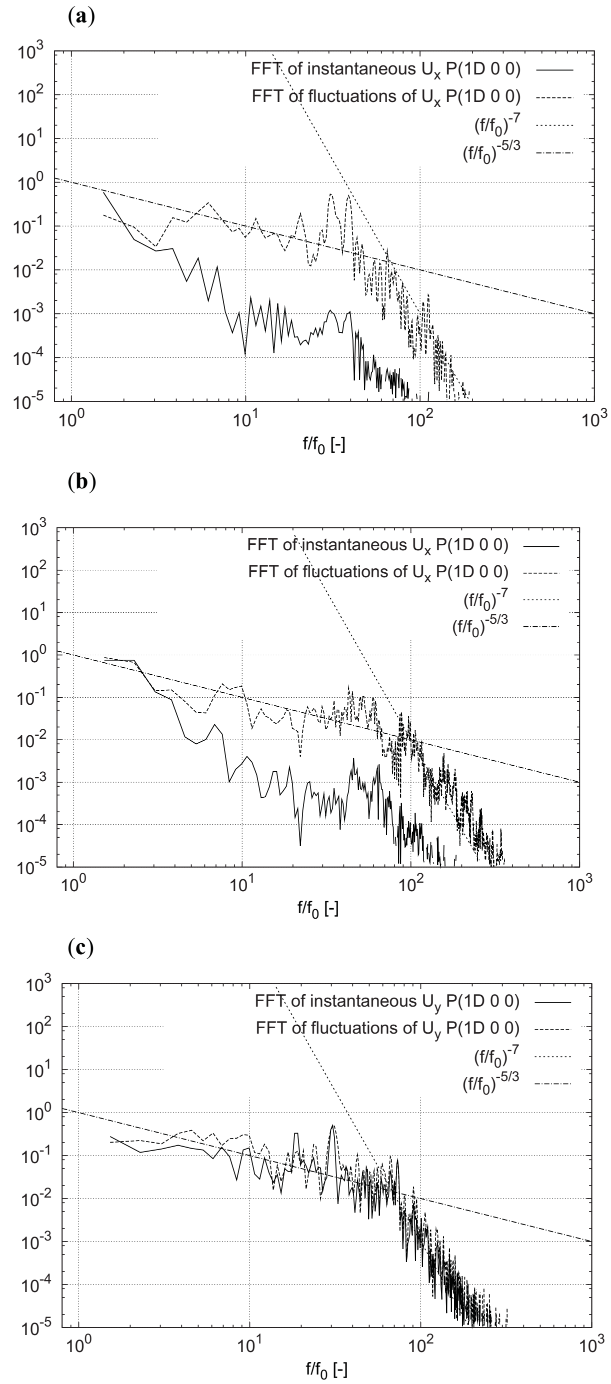

Fig. (8). Frequency spectrum obtained by Fast-Fourier transforms of the time series of velocity components and their fluctuations Ux, U'_x, Uy, U'_y and Uz, U'_z at probe point P0 (1D,0,0), inertial subrange (depicted with dash-dot line at slope angle -5/3) changes to dissipative subrange (depicted with dotted line at slope angle-7)

loss coefficient prevents the vocal folds from touching each other by the missing flow forces during the loss phase. In the five cycles, when—nevertheless—contact takes place, the maximum values of the contact pressure are lower than in the simulation without the loss coefficient. In the latter case, the maximum contact pressure values are 1.8 kPa, which is in the same range as previously reported studies (e.g.[51]). The spatial distribution of the contact pressure over time can be found in Fig. (**13**). It was found that the maximum pressures are located between the nodes 3 and 5 (for their position see Fig. **12**). Temporally, the contact pressures rise rapidly and decrease much slower depending on the position of the node. In this study, the channel between the vocal folds is very small in order to model the vocal fold impact as realistic as possible. Therefore, contact is not activated in each oscillation cycle (for example when the supraglottal flow influences the oscillation vertically so that the lateral movement is reduced).

The flow effect of the artificial loss coefficient can be seen in Fig. (**14**). Only if it is present, a complete stop of the

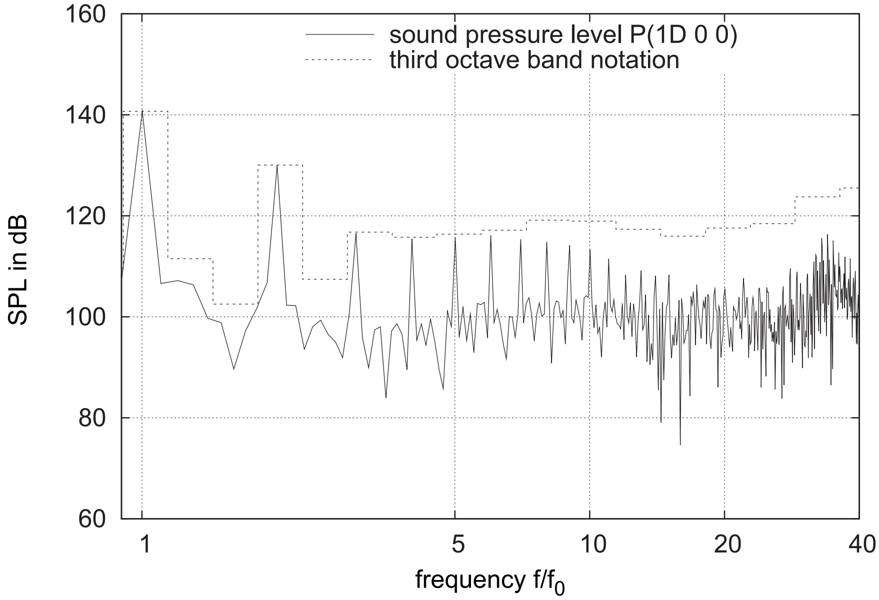

Fig. (9). Sound pressure level (SPL) (solid line) of the computed acoustic frequency spectrum at point P0 (1D,0,0) for glottal waveform, dotted lines show the third octave band notation.

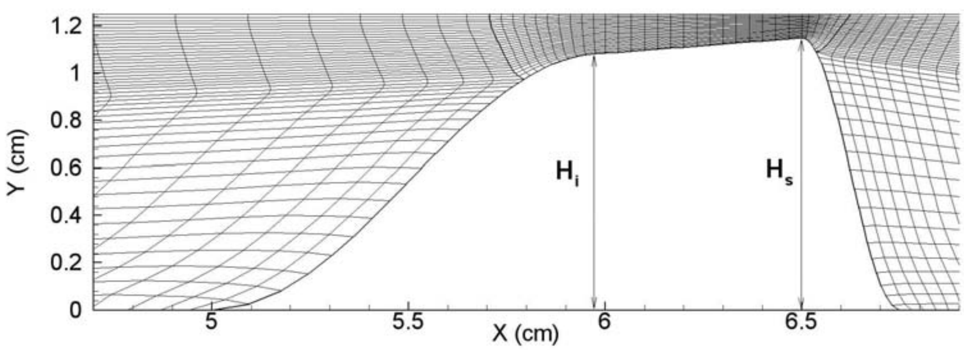

Fig. (10). Design of the oscillating vocal folds and portion of the grids.

flow is obtained. Otherwise, there is still a light flow through the constantly open channel even if the structural contact is established. A difference in the supraglottal flow field can be found in the deflecting jet, often referred to as Coanda effect. In general, the oscillation behavior of the structure is comparable in both setups in terms of oscillation frequency and oscillation form (combined lateral and torsional eigenform). So it depends on the focus of the study which approach is more adequate: For analyzing impact pressures, the simulation should be run without the artificial loss approach in order to avoid the impact energy to be affected by the decelerating effects of the flow momentum source. If the main focus is on the supraglottal flow behavior, the loss coefficient approach can be of good use since it models a real stop of the jet. It can be seen that the lateral side of the jet deflection has a higher tendency to change when the jet stops completely during vocal fold closure. It has to be noted that the flow stop has inertia effects. That means that when the loss momentum source is introduced it will take a certain time until the flow completely stops. On the flow side, the opening coefficient can be approximated using this time. It can be influenced by the dimension of the region ("glottal region" in Fig. **12**) in which the source is introduced and by the value of χ.

3.5. 2D Fluid - Structure - Acoustic Simulations

In the following we will present simulation results for a simplified geometrical model of the larynx. This simulation setup consists of a channel with the two vocal folds, which act as a constriction inside the channel as displayed in Fig. (**15a**), based on Link *et al.* [10]. Fig. (**15b**) shows the fine mesh around the vocal folds, which is necessary to accurately resolve the fluid flow. Approximately 45000 quadratic finite elements are used to resolve the fluid, which results in about 400000 degrees of freedom. For structural mechanics the vocal folds have been divided into three different layers, the body, the ligament and the cover. Each have different elasticity modulus to model the real physiology more accurately. For body, ligament and cover the elasticity moduli were set to 21 kPa, 33 kPa and 12 kPa respectively. To simulate the pressure, the lungs build up, a pressure gradient from in-- to outflow of 1.5 kPa is prescribed. The simulations show the typical self sustained

(**a**)

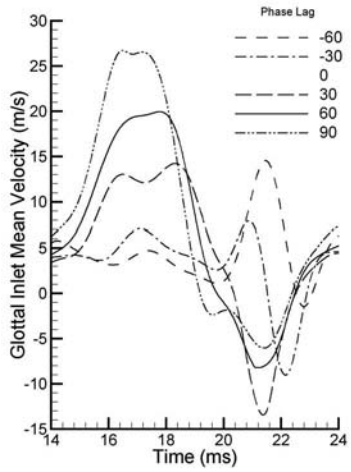

(**b**)

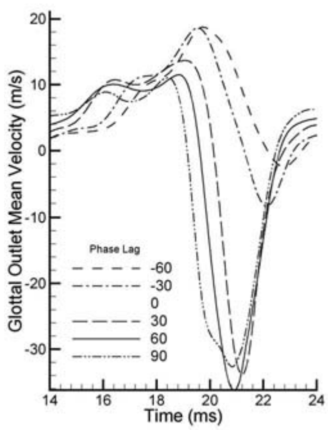

(**c**)

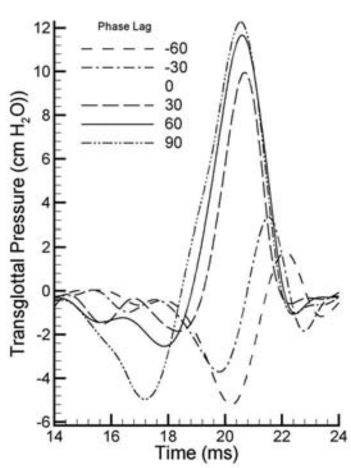

Fig. (11). Effects of phase lag on the glottal inlet and outlet velocities (**a**), (**b**) and on the tgp (**c**).

oscillation of the vocal folds during phonation, which is divided into the divergent (opening) and convergent (closing) phase as displayed in Fig. (**16**). In Fig. (**17**) the

(**a**)

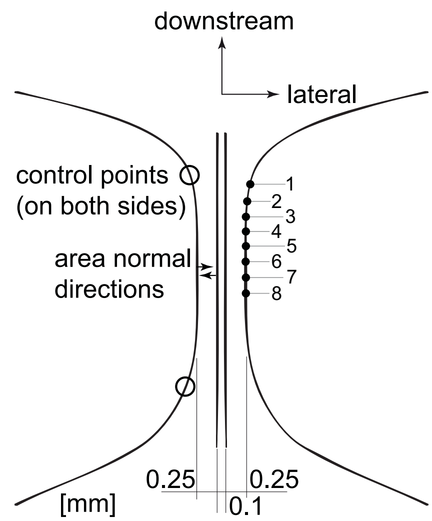

(**b**)

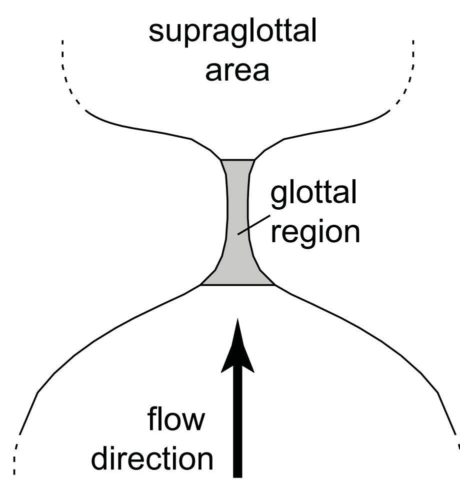

Fig. (12). Left: Position of the contact pairs in the glottal gap. Both of the pairs form a permanently open channel of 0.1 mm width between the vocal folds. Right: Position of the glottal region in the flow model in which the loss coefficient is introduced when the vocal folds distance falls below the threshold value of 0.25 mm.

fluid field can be seen at a characteristic time step. In the transient simulation one can observe, how the jet is stochastically attaching to either side of the trachea wall, which is known as the Coanda effect.

The acoustic sound computation has been separated into a computation of the flow induced sound (using Lighthill's tensor), and into a vibrational induced sound. In a series of simulations the acoustic field of vibrational and fluid induced sound was compared. As can be seen in Fig. (**18a**) the mechanical induced sound is much smaller than that of the fluid induced sound. Comparing this result with a simulation were the initial glottis width is enlarged to 0.7 mm (see Fig. **18b**) it shows that the bigger glottis results in a much broader acoustic frequency spectrum. Furthermore, no dominant frequency component is recognizable as in Fig. (**18a**) at about 190 Hz .

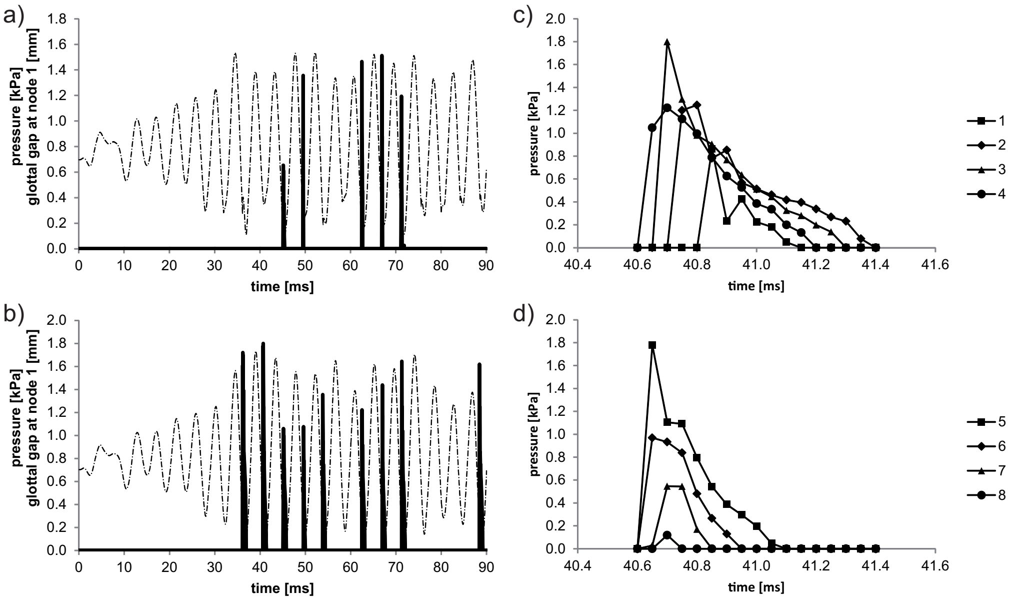

Fig. (13). Results of fluid-structure interaction simulations with contact effects: a) Width of the glottal gap (thin line) and maximum contact pressure (bold line) with artificial loss. b) Width of the glottal gap (thin line) and maximum contact pressure (bold line) without artificial loss. c) and d) Contact pressure detail over time without artificial loss at the structural nodes 1--8 as shown in Fig. **12** (left-hand side).

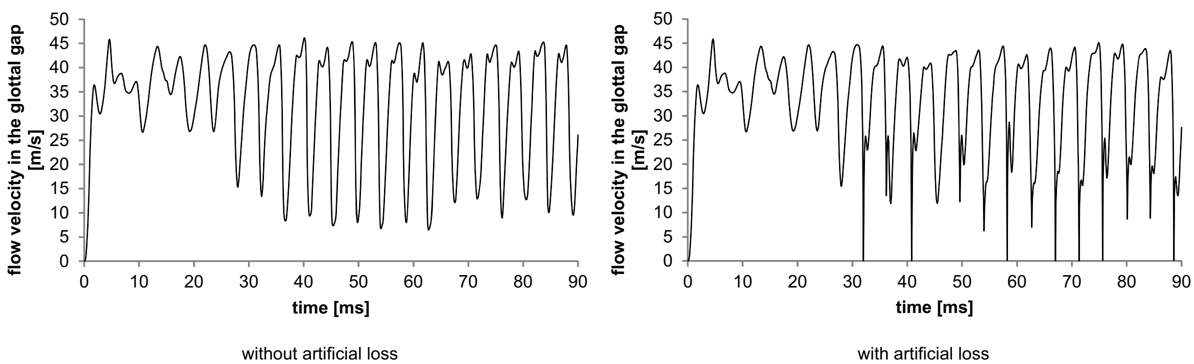

Fig. (14). Absolute air flow velocities in the middle of the glottal gap for both of the setups.

These results imply the importance of a proper closing glottis for a clear and healthy voice. Furthermore, they show that the fluid flow is the dominant source of phonation, which is hard to proof by measurements.

4. INVESTIGATION AND COMPARISON OF MODELS

A set of nineteen recent studies was selected in which finite element or other similar methods were used to model the human phonation process. A database was created listing information on modeling assumptions, geometric parameters, numerical implementation (mesh density, element types, time step size, etc.), boundary conditions and applied loads, material properties, verification procedures, analyses performed, number of parameters required to define the model, and number varied.

In some cases, the total number of applicable papers was less than 19 (e.g. only 11 studies involved fluid loading). Averages and proportions based on such cases are stated relative to their respective totals. Finally, it should be pointed out that the following averages and proportions are in regard to *reported information*, since only reported values can be tabulated.

4.1. Geometry

The vocal fold model geometry was presented graphically in all studies. In approximately half of all studies (10 of 19), the external geometry of the vocal fold model was stated specifically, and in sufficient detail to allow independent replication. Two vocal fold geometries were commonly used in vocal fold models. These included the Titze and Talkin geometry (Titze and Talkin, 1979), and the M5 geometry (Scherer *et al.,* 2001). Data on the basic geometric parameters used in vocal fold models are shown in Table **2**.

The internal geometry of the vocal folds is an important component of model definition. Vocal fold models consisted of single-layer, double-layer, and models composed of three or more layers. The numbers of models for each group was four, five, and eight, respectively, with two studies being excluded from this group. Of the 13 studies that utilized a vocal fold model consisting of two or more layers, none

(a)

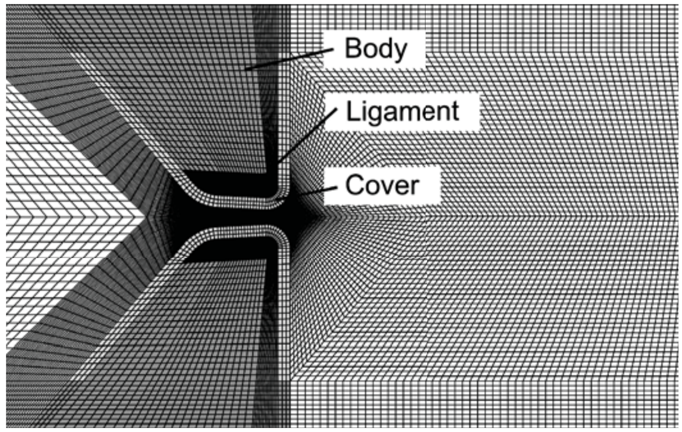

(b)

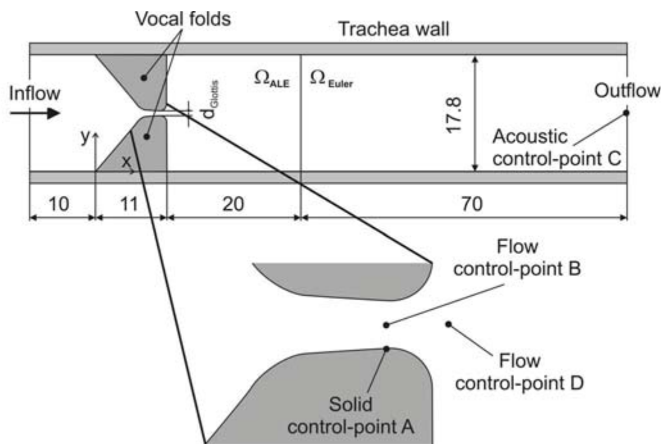

Fig. (15). Model of the larynx with vocal folds and the according mesh used for the simulations.

provided a description of the internal geometry. Of the 19 studies, six (32%) provided geometric data that was sufficiently detailed to allow independent replication of the entire model geometry. These studies all utilized single-layer models. The geometry of subglottal and supraglottal fluid domains is another critical component of model definition. The diameter and length of both the subglottal and supraglottal tracts are required since the lengths of the both tracts have been shown to have an effect on the vibratory response of the vocal folds (Thomson *et al.* [70]). Of 10 studies which utilized a fluid model component, only four provided a thorough description of the fluid geometry.

4.2. Boundary Conditions

Complete sets of structural boundary conditions were stated in 12 of 19 (63%) of all papers. Nearly all of these (11 of 12), utilized rigid, rectangular boundary conditions for the vocal fold structure, as introduced by Titze and Strong [71]. The accuracy of these boundary conditions was questioned by Hunter *et al.* [72], in which transitional regions of soft tissue were utilized to more accurately represent typical human physiology. Cook and Mongeau [73] found that boundary conditions significantly affected the vibratory characteristics of the rectangular vocal fold geometry introduced by Berry and Titze [74]. Typical fluid boundary conditions included no-slip (zero velocity) conditions at fixed walls, matched velocity at the fluid/solid interface, and prescribed pressure inlet and outlet conditions. A symmetry flow condition is also commonly applied to the centerline of the model if the fluid flow is assumed to be symmetric about the mid-sagittal plane. A total of 11 papers utilized a fluid model. Of these, 6 (55%) reported a complete set of boundary conditions. The assumption of symmetric fluid flow was utilized in 9 studies (82%).

4.3. Applied Loads

The loads applied to vocal fold models included pressure or forces applied directly to the vocal fold structure, and loads applied to inlets and/or outlets of fluid domains. Of the five studies involving loading in the absence of a fluid flow model, less than one-half provided detailed loading information. For fluid-structure interaction models, the most common loading scheme is to impose a constant pressure differential between inlet and outlet. Of the 11 studies that utilized a flow model, this type of loading was reported in 5 studies (45%). A sinusoidally varying pressure was applied to the inlet flow boundary in one study (Thomson *et al.* [70]). in total, 17 studies utilized some type of applied load (as defined above). Of these, 6 studies (35%) provided sufficiently detailed information to allow for independent replication of the load state.

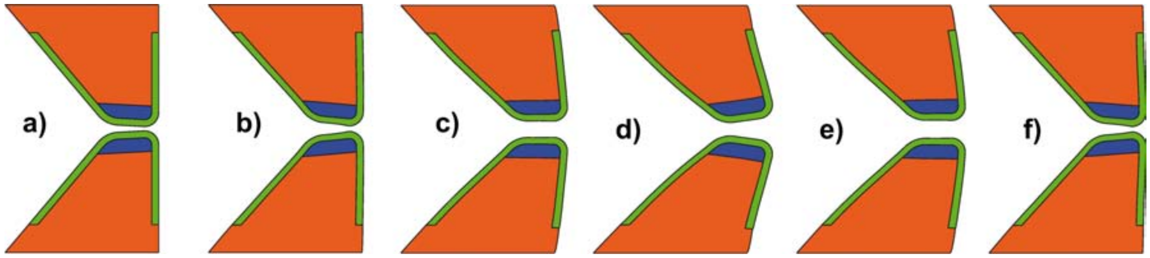

Fig. (16). Computed deformation cycle of the vocal folds, which can be divided in divergent to convergent phase.

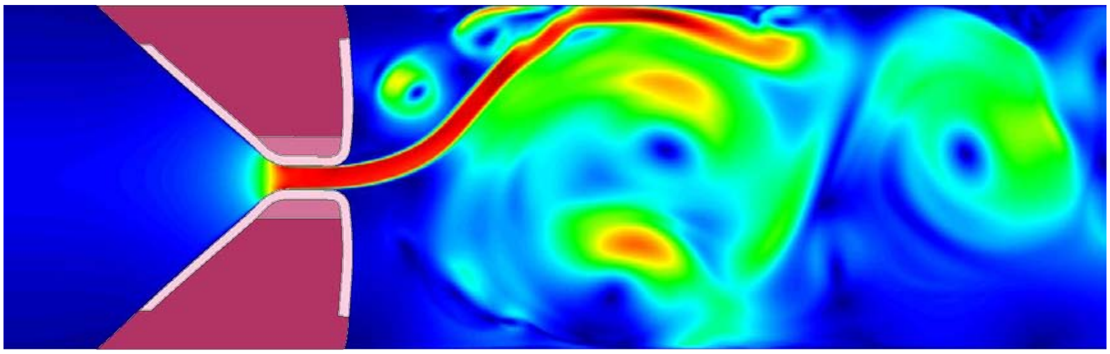

Fig. (17). Snap--shot of velocity field and deformation of vocal folds. Jet is attached to the top vocal fold --- Coanda effect.

4.4. Material Properties

A linearly elastic three layer-model of the vocal fold requires 12 structural material properties. Nonlinear models require additional parameters. Of the 18 papers that utilized a continuum vocal fold structure, eight (44%) reported a complete set of structural material properties. On average, 80% of structural properties were reported. While much progress has been made in the measurement of vocal fold tissue properties, the majority of material constants are still unmeasured (Titze, [32]). This necessitates "educated estimates" of unmeasured parameters. On average, 70% of material parameters were found to be based on ad-hoc estimates, an average of seven per study. The range of parameter values utilized in vocal fold models was examined, along with the distributions of reported values. While some parameters were found to span wide ranges, others were characterized within narrow ranges with parameter values reappearing from one study to the next. For example, more than 10 different values were reported in various studies for the transverse stiffness of the thyroarytenoid muscle, with values scattered between 2-100 kPa But the longitudinal shear modulus of the vocal ligament was assigned a value of 40 kPa in every study that has reported a value for this parameter. While the six parameters with the least variation were assigned one of 16 unique values, the six parameters with the largest variation were assigned no fewer than 39 different values. Cook *et al.* [75,76] examines the impact and influence of the material parameters and geometries. Additionally, he analyses two assumptions which reduce the number of independent parameters for the vocal fold model-the incompressibility of biological material and the planar displacement assumption. Table **3** provides a summary of material property data that has been reported in the literature. Ranges of experimentally measured tissue parameters (where available for human tissue) are provided for comparison. Table **3** represents reported data only, and is thus incomplete because (1) material property data sets are sometimes incomplete, and (2) some studies parametrically varied material parameters, but reported only extreme values. Because all reported values have been incorporated into 3, this data summarizes the material parameter ranges explored in previous studies, and provides an estimate of the number of independent values that have been used for each parameter.

4.5. Model Verification

Computational solutions should be verified for accuracy. Ideally, this is accomplished by comparison with experimental data obtained from a system closely resembling the computational model. However, since phonation models are often used precisely because tissue measurements are difficult or impossible, other methods must often be used. Computational models can be verified by comparison with published results for a similar model, or by comparison between two different numerical implementations (Berry and Titze, [77]; Alipour *et al.* [78]; Cook and Mongeau, [73]). Validation of all fluid dynamics, structural mechanics and acoustics simultaneously was done by Ruty *et al.* [79], showing a good qualitative agreement with low-order models. Cisonni [80] compared one- and two-dimensional models, especially regarding the pressure distribution and flow separation. The work of Scherer *et al.* [81,82] provides measurement data for comparison.

The model presented in Sec. 3.5 showed good agreement (see. [10]) with the experimental setup presented by Gomes *et al.* [83], in which a cylindrical body with an elastic thin plate attached to it starts to swivel due to a fluid flow from one side.

Of the 19 papers reviewed, seven (37%) reported direct quantitative comparisons with other sources. Qualitative

(a)

(b)

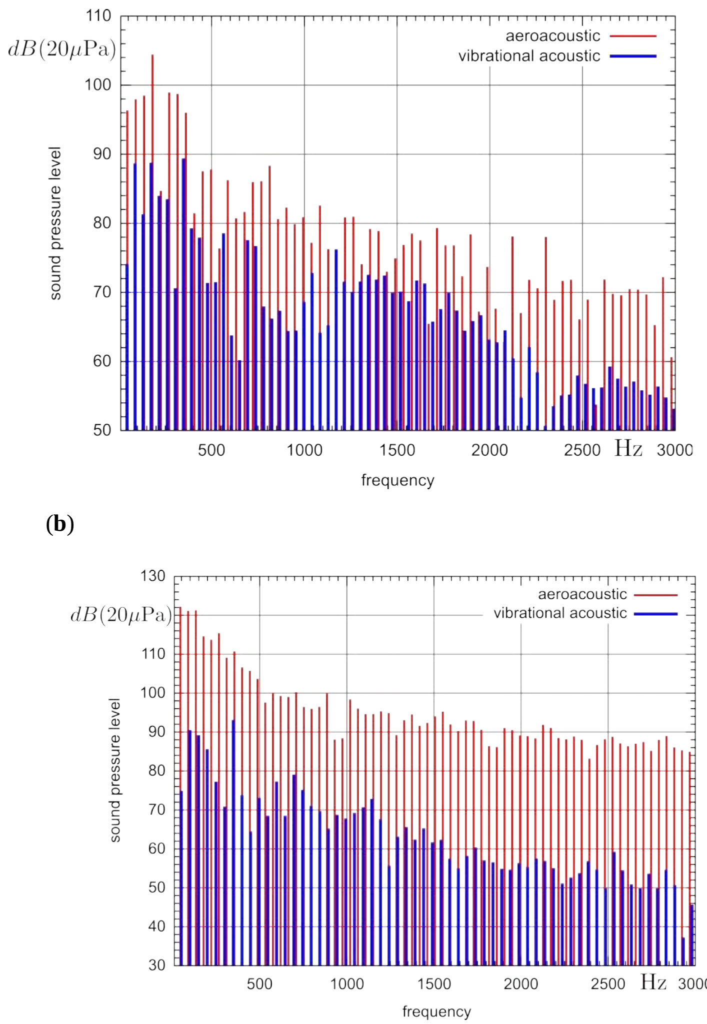

Fig. (18). Comparison of acoustic spectra for fluid induced and vibrational induced sound simulation for different glottis widths.

comparisons alone were made in eight studies (42%). Although a qualitative agreement provides some reassurance, qualitative comparisons alone are not sufficient to verify the accuracy of computational models. Some studies (21%) provided no comparison to any other published research results whatsoever.

4.6. Variation of Model Parameters

Vocal fold tissue properties have been observed to vary by several orders of magnitude (Kakita *et al.* [84]; Min *et al.* [85], Chan *et al.* [86], etc.). Systematic parametric variations are useful to assess the influence of the wide variability of measured vocal fold parameters (Berry and Titze [74]; Cook and Mongeau [73]). This approach accounts for natural variation and provides additional insight into model behavior. The total number of parameters used to define vocal fold models was found to range between 7 and 108. Typical studies utilized around 20 parameters. The percentage of parameters varied within each study ranged from 0% to 78%. However, most studies (68%) held 85% of model parameters constant throughout the study.

4.7. Reproducibility

The omission of geometric information, boundary conditions, or tissue properties may hamper independent replication. However, not all data are equally critical to the model definition. While some parameters vary from model to model, others are nearly the same for all models. All studies were examined to determine if independent replication was possible. They were divided into two categories: 1) reproducible and 2) very likely reproducible. Reproducible studies provided complete information concerning both solid and fluid domains in each the following areas: 1) model geometry, 2) material properties, 3) boundary conditions, and 4) applied loads. Very likely reproducible studies were those for which a) complete information was provided in the majority of the above categories, and b) omitted information could be obtained indirectly from the paper itself (context, allusion, or from examination of presented data), or reasonably estimated based on other similar studies (e.g. air density, tissue density, etc.). It should be noted that other important modeling topics were not included in this assessment (e.g. mesh and time step refinement, governing equations, model validation, etc.).

Table 2. Overall Dimensions Used in Computational Vocal Fold Models

	n	Minimum (mm)	Maximum (mm)	Average (mm)	Std.Dev. (mm)
Length (anterior/posterior)	10	12	17	14.9	2.0
Depth (medial/lateral)	12	4	10	9.3	1.7
Thickness (inferior/superior)	13	3.5	10.9	7.1	2.8
Cover thickness	4	0.5	1.3	1.0	0.3

Table 3. Summary of Structural Parameters Reported in Vocal Fold Modeling Studies. E – Young's Modulus; G – Shear Modulus, – Poisson's Ratio. Layers are Indicated by Subscripts: C – Cover; L – Ligament; M Thyroarytenoid Muscle. The Prime Symbol (·) Indicates Longitudinal Parameters. The Planar Displacement Assumption is Abbreviated as p.d.a

	Total Number of Values Reported	Number of Unique Values	Range of Reported Values	Experimental Range
E_c	13	8	1-- 100 kPa	4-165kPa
ν_c	12	7	0-0.76	no data
E_L	7	4	1.7-5kPa	33-78kPa2
E_L'	2	1	20kPa, p.d.a	no data
G_L'	7	1	40 kPa	no data
ν_L	7	5	0-0.68	no data
ν_L'	6	5	0-0.9	no data
E_M	14	8	2.1-36kPa	no data
E_M'	2	2	20kPa, p.d.a	2-10kPa3
G_M'	10	3	10-30kPa	no data
ν_M	14	6	0-0.47	no data
ν_M'	7	4	0-0.9	no data

Following the above guidelines, only three studies (16%) were deemed to be reproducible and another four were deemed to be partially reproducible. These findings may be generalized by concluding that 37% of all studies could reasonably be replicated by independent researchers. The reasons for exclusion from this group were remarkably consistent. Lack of geometric information was found in all remaining studies, a lack of applied loading information found in 83%, and lack of complete material properties sets in 75% of these studies. Structural boundary conditions were almost always stated (see Section IV.B), but fluid boundary conditions were omitted in 4 of 8 non-reproducible studies that utilized a fluid model (50%). An overview of reproducibility of different parameters in reviewed studies is listed in Table **4**.

4.8. Discussion

A great deal of valuable information may be obtained through the use of finite element vocal fold models, much of which could not be gleaned as effectively using any other methods. The use of finite element methods allows systematic variation of parameters, which cannot be accomplished clinically. The finite element method may provide a more complete understanding of the deformation field and the stress state of the human vocal folds, thus eventually contributing to improved clinical treatment and surgical intervention methods.

Any lack of rigor may hamper progress in future computational efforts. For example none of the vocal fold models reviewed in this study reported the internal geometry of the model. This may be related to the fact that no standard internal and external vocal fold geometry has been developed based on measurements of actual vocal folds. Boundary conditions follow a similar pattern. Nearly all

Table 4. Overall Reproducibility Rates from Reviewed Studies (n = 19). The First Four Rows Address Model Definition Issues, While the Last Four Rows Address Numerical Implementation Issues. Fluid and Solid Domains Indicated by (f) and (s) Respectively

Aspect	Percentage Reproducible
Geometry	37% (s) 45% (f)
Boundary Conditions	63%
Loading	35 %
Material Properties	44 % (s) 55 % (f)
Mesh Convergence	20 %
Time Step Convergence	25 %
Element Type Reported	77 %
Quantitative Verification	37 %

vocal fold models incorporate the rigid boundary conditions of Titze and Strong [71], although the actual impedance of the vocal folds supports has never been measured. Applied loads are fairly well documented, in particular the transglottal pressure drop (Hirano [87], Holmberg *et al.* [88]; Scherer *et al.* [89]). Virtually all computational studies involving fluid-structure interactions were observed to utilize information from such studies. The material properties of vocal fold tissue, on the other hand, are not very well known. Most studies utilized all available measured values, but researchers are compelled to estimate a number of unknown parameters. The utilization of previously estimated parameters allows comparisons with previous research, but does not expand the range or distribution of estimated values. Perhaps the most rigorous approach would be to utilize previously assumed values for validation and comparison with previous studies, and then investigate other reasonable values for each parameter. This would provide valuable information on the influence of each parameter, and offer expanded sets of estimated parameter values for subsequent studies.

5. CONCLUSION

We have presented an overview about the current state of mathematical models for the human phonation process. Therewith, we have discussed the different contributions based on multi-mass and PDE based models. The obtained simulation results provide a better understanding of the human phonation and will developed in future to valuable tools allowing surgical planning, diagnostics, and rehabilitation evaluations on an individual basis. To achieve this outlook, effort has to be put into reducing the simulation time. This may either by done by simplification as the multi-mass model or improving algorithms and implementations to make a fully coupled 3D simulation in acceptable time possible. Furthermore, realistic geometries and material properties need to be determined to achieve reliable simulations.

ACKNOWLEDGEMENT

This work was supported by Deutsche Forschungsgemeinschaft Grant No. FOR894/2 *Stromungsphysikalische Grundlagen der menschlichen Stimmgebung*, FWF grant I532-N20 and DFG grant BU 2231/2-1.

REFERENCES

[1] Flanagan J, Landgraf L. Self-oscillating source for vocal-tract synthesizers. Audio Electroacoust IEEE Trans 1968; 16(1): 57-64.

[2] Titze IR. The Human Vocal Cords: A Mathematical Model, Part I. Phonetica 1973; 28: 129-70.

[3] Koizumi T, Taniguchi S, Hiromitsu S. Two-mass models of the vocal cords for natural sounding of voice synthesis. J Acoust Soc Am 1987; 82: 1179-92.

[4] Kob M. Physical modeling of the singing voice. University of Technology Aachen, PhD thesis, 2002.

[5] Alipour F, Berry DA, Titze IR. A finite-element model of vocal-fold vibration. J Acoust Soc Am 2000; 108: 3003-12.

[6] Tao C, Jiang J, Zhang Y. Simulation of vocal fold impact pressures with a self-oscillating finite element model. J Acoust Soc Am 2006; 119: 3987-94.

[7] Rosa MO, Pereira JC, Grellet M, Alwan A. A contribution to simulating a three-dimensional larynx model using the finite-element method. J Acoust Soc Am 2003; 114(5): 2893-905.

[8] Zhao W, Frankel SH, Mongeau L. Numerical simulation of sound from confined pulsating axisymmetric jets. AIAA J 2001; 39: 1869-74.

[9] Bae Y, Moon Y. Computation of Phonation aeroacoustics by an INS/PCE splitting method. Computers & Fluids2008; 37: 1332-43.

[10] Link G, Kaltenbacher M, Breuer M, Döllinger M. A 2D finite-element scheme for fluid-solid-acoustic interactions and its application to human phonation. Comp Methods Appl Mech Eng 2009; 198: 3321-34.

[11] Ishizaka K, Flanagan JL. Synthesis of voiced sounds from a two-mass model of the vocal cords. BLTJ 1972; 51: 1233-68.

[12] Stevens K. Physics of laryngeal behavior and larynx mode. Phonetica 1977; 34: 264-79.

[13] Titze I. The physics of small-amplitude oscillation of the vocal folds. J Acoust Soc Am 1988; 83: 1536-52.

[14] Ishizaka K, Isshiki N. Computer simulation of pathological vocal-cord vibration. J Acoust Soc Am 1976; 60: 1193-98.

[15] Steinecke I, Herzel H. Bifurcations in an asymmetric vocal fold model. J Acoust Soc Am 1995; 97: 1571-8.

[16] Döllinger M, Hoppe U, Hettlich F, Lohscheller J, Schuberth S, Eysholdt U. Vibration parameter extraction from endoscopic image series of the vocal fold. IEEE Trans Biomed Eng 2002; 49: 773-81.

[17] Story B, Titze I. Voice simulation with a body-cover model of the vocal folds. J Acoust Soc Am 1995; 97: 1249-60.

[18] Hirano M. Morphological structure of the vocal cord as a vibrator and its variations. Folia Phonatrica 1974; 26: 89-94.

[19] Hirano M, Kakita Y. Cover-body theory of vocal cord vibration. In Daniloff RG. (Ed.) Speech Science, College Hill Press, San Diego. 1985; p. 1-46.

[20] Titze I, Story B. Rules for controlling low-dimensional vocal fold models with muscle activation. J Acoust Soc Am 2002; 112: 1064-76.

[21] Adachi S, Yu J. Two-dimensional model of vocal fold vibration for sound synthesis of voice and soprano singing. J Acoust Soc Am 2005; 117: 3213-24.

[22] Childers D, Hicks D, Moore G, Alsaka Y. A model for vocal fold vibratory motion, contact area, and electroglottogr. Am J Acoust Soc Am 1986; 80: 1309320.

[23] Lous N, Hofmans G, Veldhuis R, Hirschberg A. A symmetrical two mass vocal fold model coupled to vocal tract and trachea, with application to prothesis design. Acta Acustica 1998; 84: 1135-50.

[24] Lucero JC. The minimum lung pressure to sustain vocal fold oscillation. J Acoust Soc Am 1995; 98: 779-84.

[25] Lucero JC. A theoretical study of the hysteresis phenomenon at vocal fold oscillation onset-offset. J Acoust Soc Am 1999; 105(1): 423-31.

[26] Lucero JC, Koenig LL. On the relation between the phonation threshold lung pressure and the oscillation frequency of the vocal folds (L) [Article]. J Acoust Soc Am 2007; 121(6): 3280-3.

[27] Laje R, Gardner T, Mindlin GB. Continuous model for vocal fold oscillations to study the effect of feedback. Phys Rev E 2001; 64(5): 056201.

[28] Avanzini F. Simulation of vocal fold oscillation with a pseudo-one-mass physical model. Speech Commun 2008; 50: 95-108.

[29] Drioli C. A flow waveform-matched low-dimensional glottal model based on physical knowledge. J Acoust Soc Am 2005; 117(5): 3184-95.

[30] Titze I. The human vocal cords: A mathematical model, part II. Phonetica 1974; 29: 1-21.

[31] Wong D, Ito M, Cox N, Titze I. Observation of perturbation in a lumped-element model of the vocal folds with application to some pathological cases. J Acoust Soc Am 1991; 89: 383-94.

[32] Titze I. Myoelastic Arodynamic Theory of Phonation. Iowa City, IA: National Center for Voice and Speech. 2006.

[33] Berge P, Pomeau Y, Vidal C. Order within Chaos: Towards a deterministic approach to turbulence. New York: Wile. 1984.

[34] JC L. Optimal glottal configuration for ease of phonation. J Voice 1998; 12: 151-8.

[35] Pelorson X, Hirschberg A, van Hassel R, Wijnands A, Auregan Y. Theoretical and experimental study of quasi-steady flow separation within the glottis during phonation. J Acoust Soc Am 1994; 96: 3416-31.

[36] Sciamarella D, d'Alessandro C. On the acoustic sensitivity of a symmetrical two-mass model of the vocal folds to the variation of control parameters. Acta Acustica 2004; 90: 746-61.

[37] Tao C, Zhang Y, Hottinger DG, Jiang JJ. Asymmetric airflow and vibration induced by the Coanda effect in a symmetric model of the vocal folds. J Acoust Soc Am 2007; 122(4): 2270-8.

[38] de Vries MP, Schutte HK, Veldman AEP, Verkerke GJ. Glottal flow through a two-mass model: Comparison of Navier-Stokes solutions with simplified models. J Acoust Soc Am 2002; 111(4): 1847-5.
[39] Alipour F, Scherer RC. Flow separation in a computational oscillating vocal fold model. J Acoust Soc Am 2004; 116: 1710-9.
[40] Decker G, Thomson S. Computational Simulations of Vocal Fold Vibration: Bernoulli Versus Navier-Stokes. J Voice 2007; 21: 273-84.
[41] Sciamarella D, Quere PL. Solving for unsteady airflow in a glottal model with immersed moving boundaries. Eur J Mech B/Fluids 2008; 27: 42-53.
[42] Thomson SL, Mongeau L, Frankel SH. Physical and numerical flow-excited vocal fold models. In: 3rd International Workshop MAVEBA. Firenze University Press 2003; p. 147-50. ISBN 88-8453-154-3.
[43] Luo H, Mittal R, Zheng X, Bielamowicz SA, Walsh RJ, Hahn JK. An immersed-boundary method for flow-structure interaction in biological systems with application to phonation. J Comput Phys 2008; 227: 9303-32.
[44] Coanda H. Device for deflecting a stream of elastic fluid projected into an elastic fluid. US-patent 1935; 2.052.869.
[45] Erath BD, Plesniak MW. The occurrence of the Coanda effect in pulsatile flow through static models of the human vocal folds. J Acoust Soc Am 2006; 120(2): 1000-11.
[46] Zhao W, Zhang C, Frankel SH, Mongeau L. Computational aeroacoustics of phonation, Part I: Computational methods and sound generation mechanisms. J Acoust Soc Am 2002; 112: 2134-46.
[47] Zhang Z, Mongeau L, Franke SH, Thomson SL. Sound generation by steady flow through glottisshaped orifices. J Acoust Soc Am 2004; 116: 1720-8.
[48] Williams JEF, Hawkings DL. Sound generation by turbulence and surface in arbitrary motion. Philosophical Transactions of the Royal Society of London, Series A, Mathematical and Physical Sciences. 1969; 264: 321-42.
[49] Suh J, Frankel SH. Numerical simulation of turbulence transition and sound radiation for flow through a rigid glottal model. J Acoust Soc Am 2007; 121(6): 3728-39.
[50] Krane MH. Aeroacoustic production of low-frequency unvoiced speech sounds. J Acoust Soc Am 2005; 118: 410-27.
[51] Gloerfelt X, Lafon P. Direct Computation of the noise induced by a turbulent flow through a diaphragm in a duct at low Mach number. Computers & Fluids 2008; 37: 388-401.
[52] Horáček J, Šidlof P, Švec JG. Numerical simulation of self-oscillations of human vocal folds with Hertz model of impact forces. J Fluid Struct 2005; 20: 853-69.
[53] Horáček J, Laukkanen AM, Šidlof P. Estimation of impact stress using an aeroelastic model of voice production. Logop Phoniatr Vocol 2007; 32: 185-92.
[54] Decker GZ, Thomson SL. Computational simulations of vocal fold vibration: Bernoulli Versus Navier-Stokes. J Voice 2007; 21: 273-84.
[55] Zheng X, Xue Q, Mittal R, Beilamowicz S. A coupled sharp-interface immersed boundary-finite-element method for flow-structure interaction with application to human phonation. J Biomech Eng 2010; 132(11): 111003.
[56] Belytschko T, Liu WK, Moran B. Nonlinear Finite Elements for Continua and Structures. Chichester: J. Wiley & Sons Ltd; 2000.
[57] Seo JH, Mittal R. A high-order immersed boundary method for acoustic wave scattering and low-Mach number flow-induced sound in complex geometries. J Comput Phys 2011; 230: 1000-19.
[58] Tokuda I, Horáček J, Švec J, Herzel H. Comparison of biomechanical modeling of register transitions and voice instabilities with excised larynx experiments. J Acoust Soc Am 2007; 122: 519-31.
[59] van den Berg J, Tan T. Results of experiments with human larynxes. Pract Otorhinolaryngol (Basel) 1959; 21: 425-50.
[60] van den Berg J. Sound productions in isolated human larynges. Annals of New York Academy of Sciences 1968; 155: 18-27.
[61] Horáček J, Švec J, Veselý J, Vilkman E. Bifurcations in excised larynges caused by vocal fold elongation. In Giovanni A, Dejonckere P, Ouaknine M, (Eds.). Proc Int Conf Voice Physiol Biomech 2004; p. 87-89.
[62] OpenCFD Ltd. OpenFOAM1.5 documentation; http://www.openc-fd.co.uk/openfoam/doc/index.html.
[63] Kaltenbacher M, Escobar M, Ali I, Becker S. Numerical simulation of flow-induced noise using LES/SAS and Lighthill's Acoustics Analogy. Intl J Numerical Methods Fluids 2010; 63(9): 1103-22.
[64] Kaltenbacher M. Advanced simulation tool for the design of sensors and actuators. In: Proceedings of Eurosensors XXIV. Linz, Austria, 2010; CD-ROM.
[65] Triep M, Brücker C, SchröderW. High-speed PIV measurements of the flow downstream of a dynamic mechanical model of the human vocal folds. Experiments Fluids 2005; 39(2): 232-45.
[66] Mattheus W, Zörner S, Kaltenbacher M, Schwarze R, Brücker C. Vortex induced sound in a pulsating flow through an elliptic glottal shaped constriction. Eur J Mech B/Fluids (In review).
[67] Schwarze R, MattheusW, Klostermann J, Brücker C. Starting jet flows in a three-imensional channel with larynx-shaped constriction. Computers & Fluids (submitted).
[68] Zheng X, Bielamowicz S, Luo H, Mittal R. A computational study of the effect of false vocal folds on glottal flow and vocal fold vibration during phonation. J Biomed Eng Soc 2009; 37: 625-42.
[69] Simo JC, Laursen TA. An augmented Lagrangian treatment of contact problems involving friction. Comput Struct 1992; 42: 97-116.
[70] Thomson SL, Mongeau L, Frankel SH. Aerodynamic transfer of energy to the vocal folds. J Acoust Soc Am 2005; 118(3): 1689-100.
[71] Titze IR, Strong WJ. Normal modes in vocal cord tissues. J Acoust Soc Am 1975; 57(3): 736-44.
[72] Hunter EJ, Titze IR, Alipour F. A three-dimensional model of vocal fold abduction/adduction. J Acoust Soc Am 2004; 115: 1747-59.
[73] Cook DD, Mongeau L. Sensitivity of a continuum vocal fold model to geometric parameters, constraints, and boundary conditions. J Acoust Soc Am 2007; 121(4): 2247-53.
[74] Berry DA, Titze IR. Normal modes in a continuum model of vocal fold tissues. J Acoust Soc Am 1996; 100(5): 3345-54.
[75] Cook DD, Nauman E, Mongeau L. Reducing the number of vocal fold mechanical tissue properties: Evaluation of the incompressibility and planar displacement assumptions. J Acoust Soc Am 2008; 124(6): 3888-96.
[76] Cook DD, Nauman E, Mongeau L. Ranking vocal fold model parameters by their influence on modal frequencies. J Acoust Soc Am 2009; 126(4): 2002-10.
[77] Alipour F, Titze IR. Combined simulation of airflow and vocal fold vibrations, in Vocal Fold Physiology, Controlling Complexity and Chaos. Singular Publishing Group, San Diego. 1996; p. 17-29.
[78] Alipour F, Scherer R. Vocal fold bulging effects on phonation using a biophysical computer model. J Voice 2000; 4(14): 470-83.
[79] Ruty N, Pelorson X, Hirtum AV, Lopez-Arteaga I, Hirschberg A. An *in vitro* setup to test the relevance and the accuracy of low-order vocal folds models. J Acoust Soc Am 2007; 121(1): 479-90.
[80] Cisonni J, Hirtum AV, Luo X, Pelorson X. Experimental validation of quasi-one-dimensional and two-dimensional steady glottal flow models. Med Biol Eng Comput 2010; 48: 903-10. 10.1007/s11517-010-0645-7.
[81] Scherer RC, Titze IR, Curtis JF. Pressure-flow relationships in two models of the larynx having rectangular glottal shapes. J Acoust Soc Am 1983; 73(2): 668-76.
[82] Fulcher LP, Scherer RC, Witt KJD, Thapa P, Bo Y, Kucinschi BR. Pressure distributions in a static physical model of the hemilarynx: Measurements and computations. J Voice 2010; 24(1): 2-20.
[83] Gomes JP, Lienhart H. Experimental study on a fluid-structure interaction reference test case. In Fluid-Structure Interaction - Modelling, Simulation, Optimization. 2006.
[84] Kakita Y, Hirano M, Ohmaru K. Physical properties of the vocal fold tissue. In: Vocal Fold Physiology; 1981.
[85] Min YB, Titze IR, Alipour-Haghighi F. Stress-strain response of the human vocal ligament. Ann Otol Rhinol Laryngol 1995; 104: 563-9.
[86] Chan RW, Titze IR. Viscoelastic shear properties of human vocal fold mucosa: Measurement methodology and empirical results. J Acoust Soc Am 1999; 106: 2008-21.
[87] Hirano M. Clinical Examination of Voice: Disord Human Commun 1981; p. 100.
[88] Holmberg EB, Hillman RE, Perkell JS. Glottal airflow and transglottal air pressure measurements for male and female speakers in soft, normal, and loud voice. J Acoust Soc Am 1988; 84(2): 511-29.

[89] Alipour F, Scherer RC. Effects of oscillation of a mechanical hemilarynx model on mean transglottal pressures and flows. J Acoust Soc Am 2001; 110(3): 1562-9.

[90] Tao C, Zhang Y, Hottinger DG, Jiang JJ. Asymmetric airflow and vibration induced by the Coanda effect in a symmetric model of the vocal folds. J Acoust Soc Am 2007; 122: 2270-8.

Received: November 25, 2010 Revised: February 02, 2011 Accepted: February 05, 2011